Electronic Supplementary Material (ESI) for Nanoscale.

Electrocatalysis of polysulfide conversion by conductive RuO_2 Nano Dots for lithium–sulfur batteries

Ruxing Wang,[a] Kangli Wang,*[,a] Shu Gao, [b] Mao Jiang, [b] Jing Han, [b] Min Zhou, [a] Shijie Cheng, [a] Kai Jiang,*[a]

[a]*State Key Laboratory of Advanced Electromagnetic Engineering and Technology, School of Electrical and Electronic Engineering, Huazhong University of Science and Technology, Wuhan, Hubei 430074, China*

[b]*State Key Laboratory of Materials Processing and Die & Mould Technology, School of Materials Science and Engineering, Huazhong University of Science and Technology, Wuhan, Hubei 430074, China.*

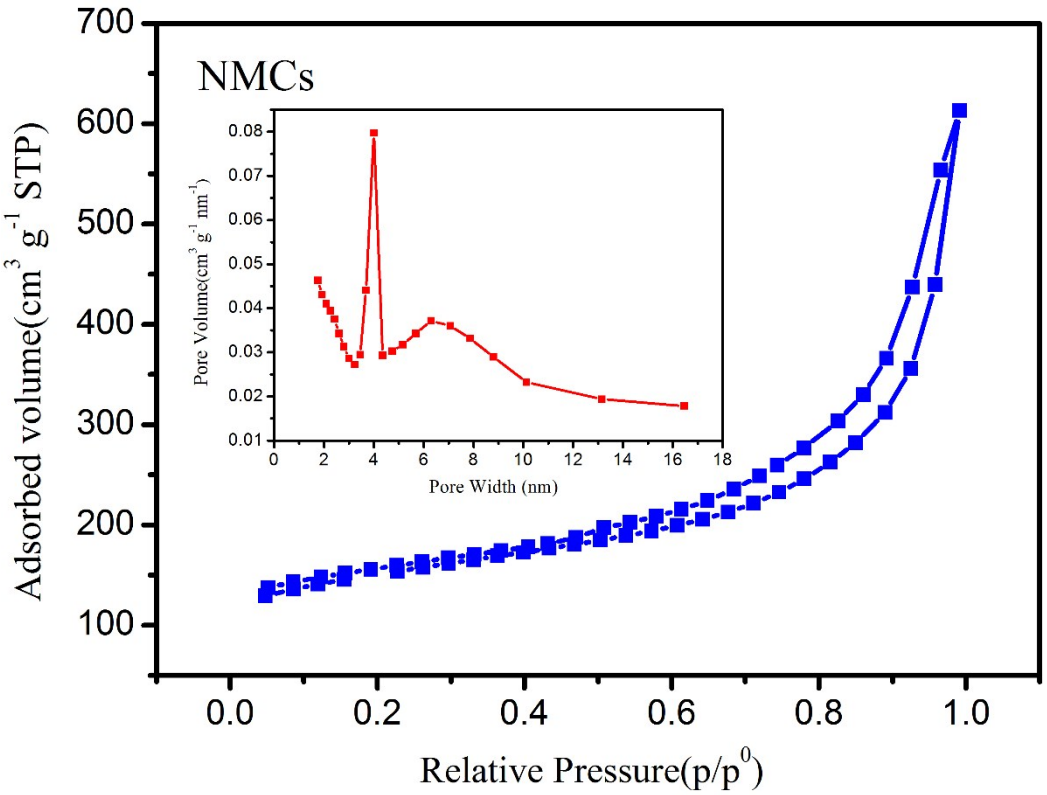

Figure S1. The nitrogen adsorption/desorption curves and pore diameter distributions of the NMCs composite.

Crystal size calculation: Based on the Debye Scherrer equation $D = \kappa\lambda/B_{1/2}\cos\theta$, the crystal size of RuO_2 are calculated to be $D_{(110)} = 5.9\ nm$, $D_{(101)} = 9.3\ nm$, $D_{(211)} = 7.4\ nm$. The particle size calculated by the Sherrer formula from the XRD patterns shows a small difference compared with the TEM images, which may attributed to differences on test equipment, instrumental error and the existence of a certain degree of particle size distribution.

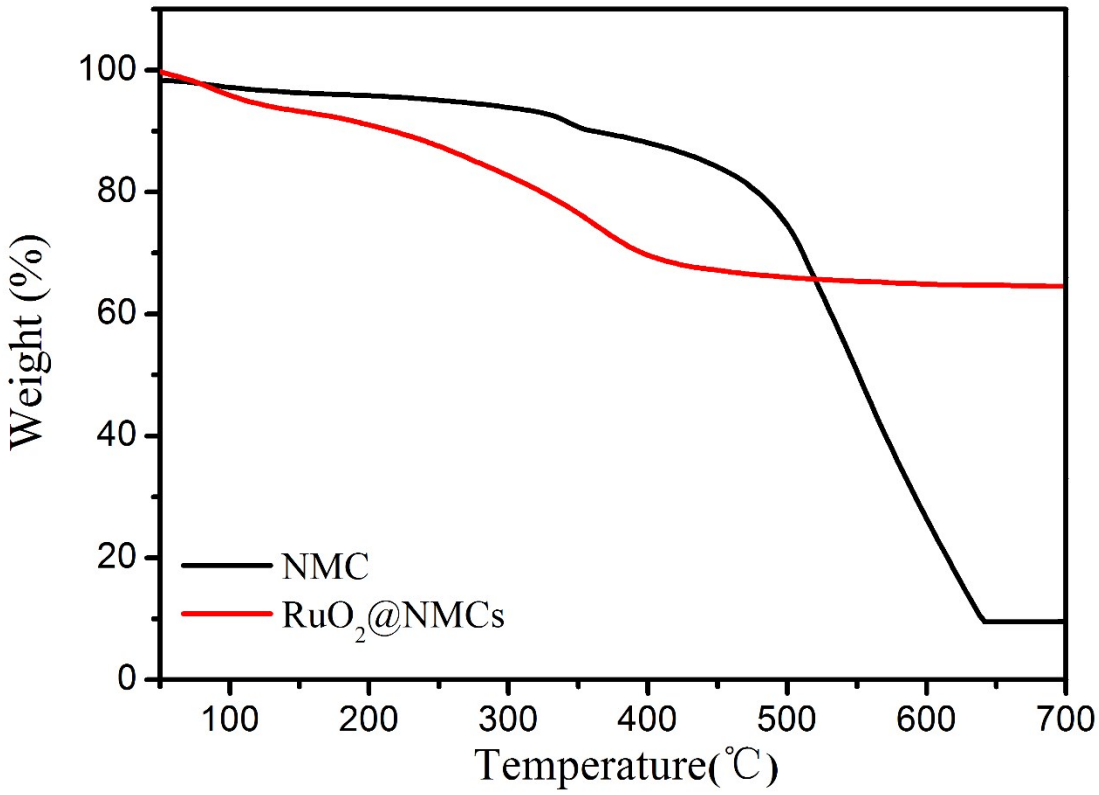

Figure S2. TGA curves of the NMCs and RuO_2@NMCs composites.

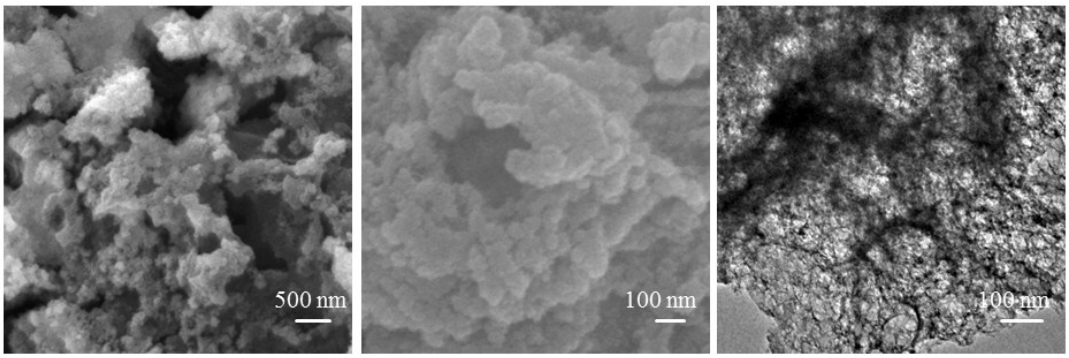

Figure S3. SEM and TEM images of NMCs/S

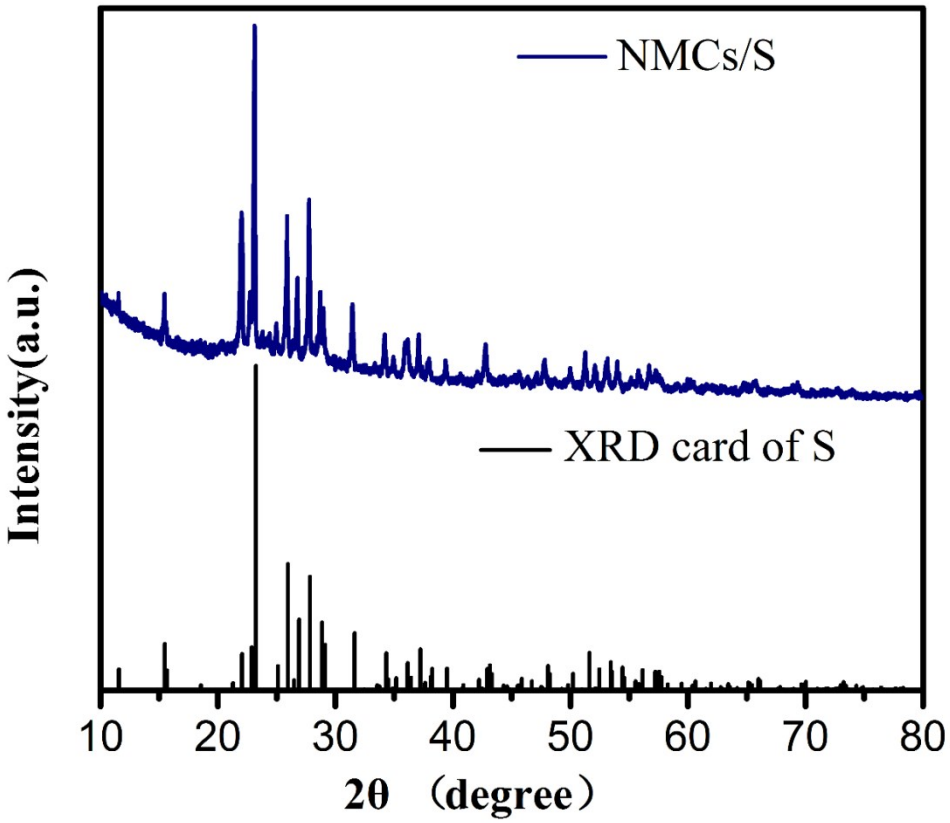

Figure S4. XRD patterns of the as-prepared NMCs/S with the corresponding PDF standard card.

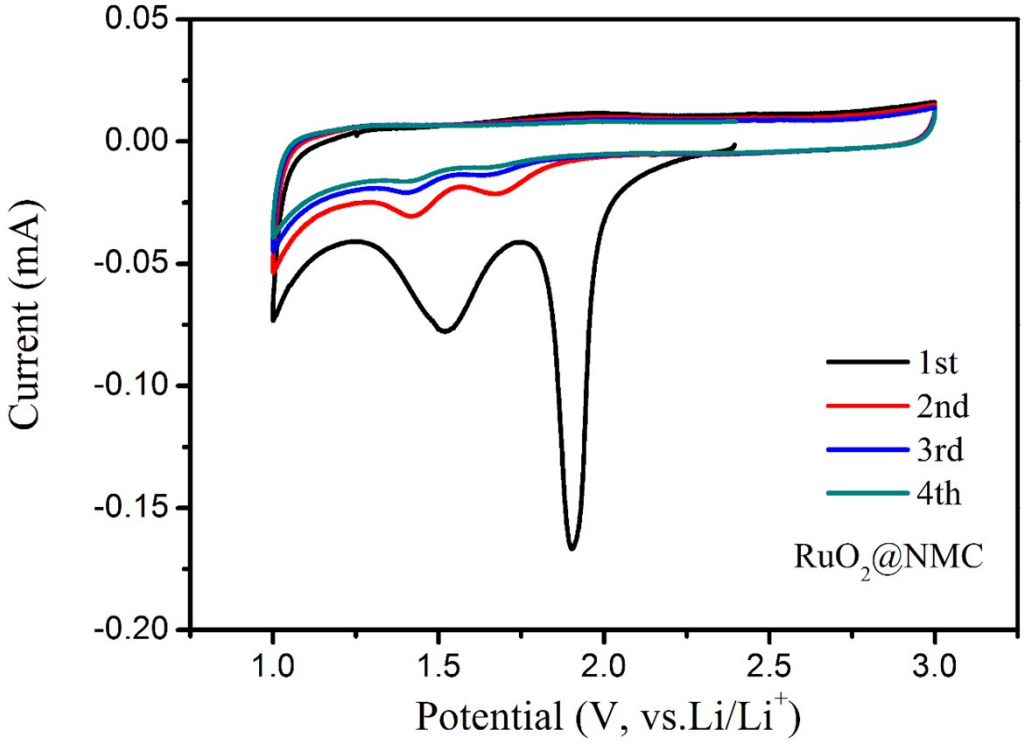

Figure S5. CV curves of the initial four cycles of the RuO_2@NMC cathode at a scan rate of 0.1

mV s^{-1}.

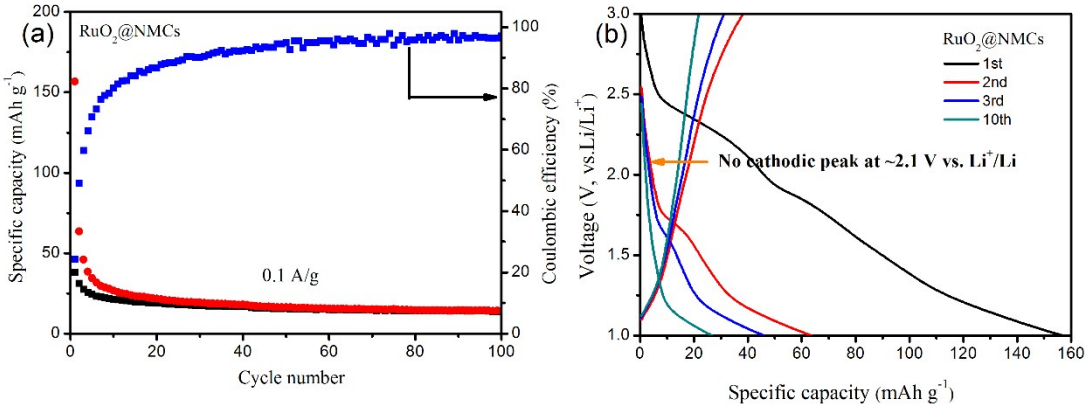

Figure S6. (a) Cycle performances of the RuO_2@NMCS electrode at 0.1 A/g. (b) Charge and discharge curves of the RuO_2@NMCs electrode.

The illustration of the fitting unit of the equivalent circuits for EIS fitting: The EIS spectra are composed of a depressed semicircle in the high frequency region and a long inclined line in the low frequency before cycling, corresponding to the charge-transfer process (R_{ct}) and a semi-infinite Warburg diffusion process, respectively. The intercept at high frequency is associated with the combination resistances (Rs) constituted by ionic resistance of electrolyte, the intrinsic resistance of active materials, and some contact resistances between active materials and current collectors. After the first cycle, a new semicircle in the medium frequency appeared, which is related to the formation of an insulating layer of lithium sulfide (Li_2S) on the host matrix in the cathode and probably the gradual build-up of solid-electrolyte interphase (SEI) resistance (*Re*)

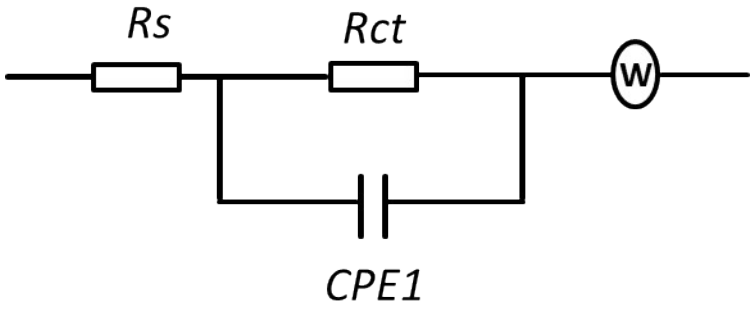

Figure S7. The equivalent circuits for EIS fitting before cycling test

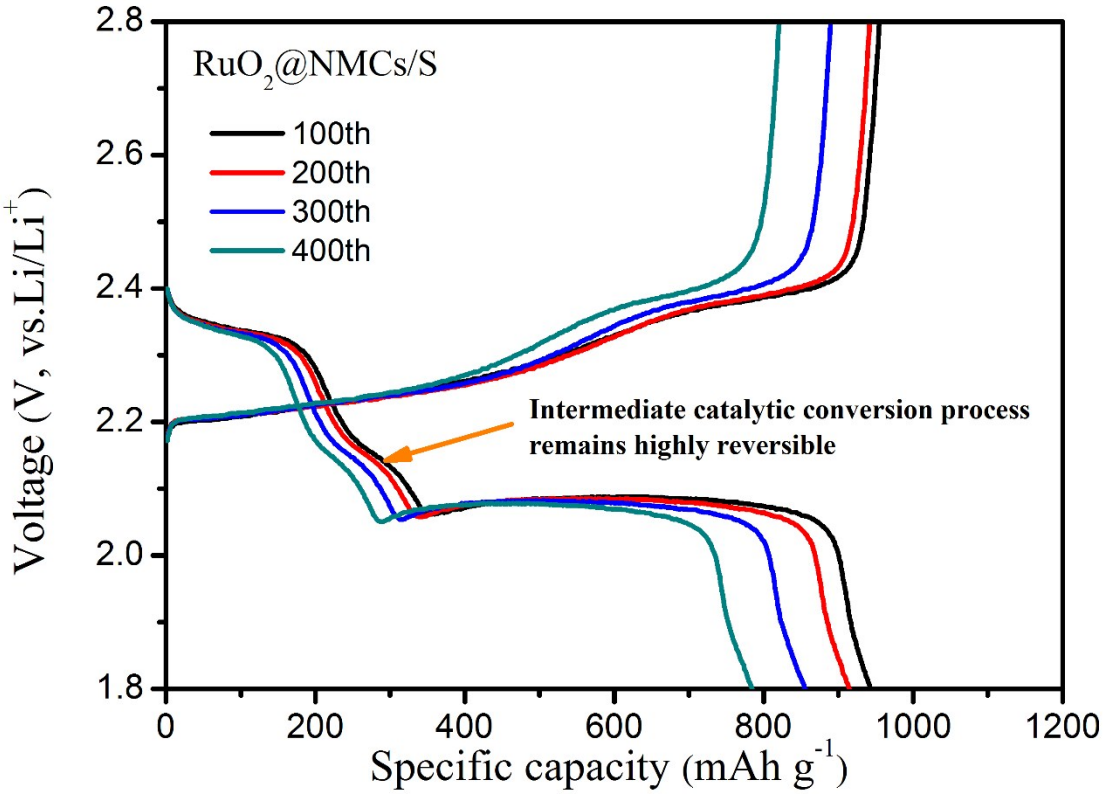

Figure S8. Charge-discharge profiles of the RuO_2@NMCs/S composite at 0.5C in 100, 200, 300 and 400 cycles.

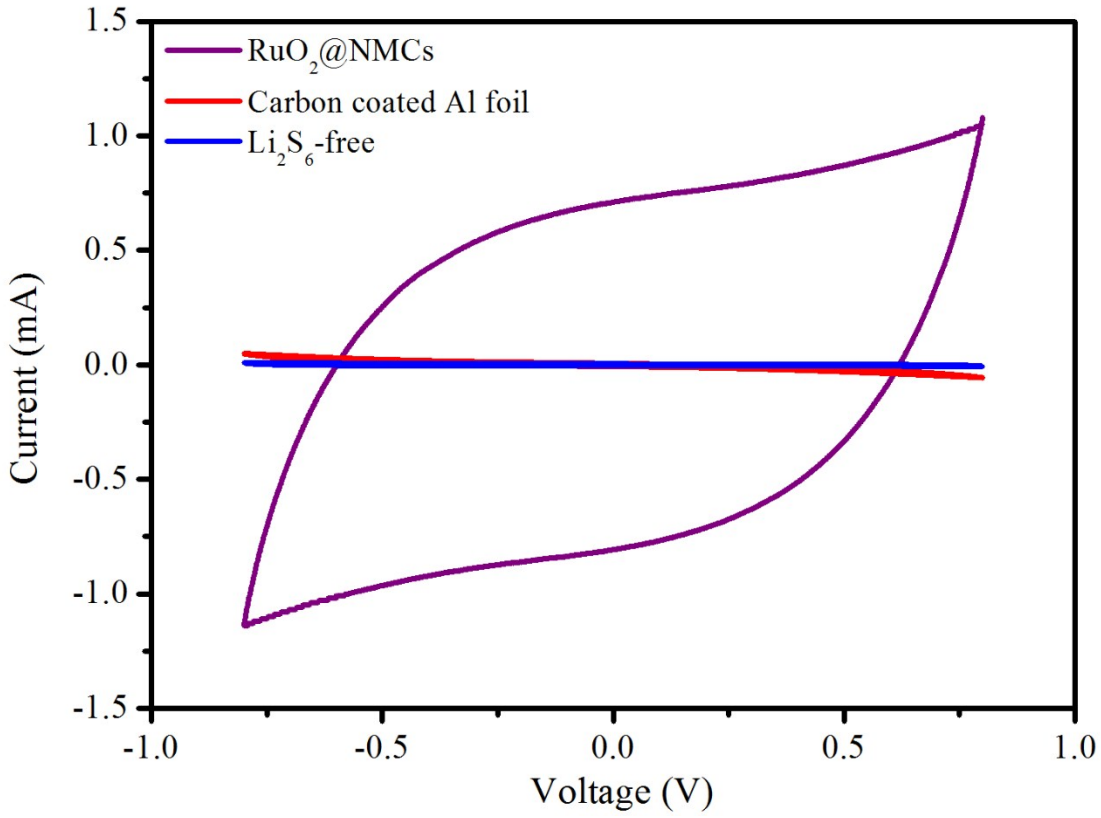

Figure S9. Cyclic voltammograms of symmetric cells of RuO_2@NMCs, Carbon coated aluminum foil electrodes with and without Li_2S_6.

Synthesis details of Li_2S_6 and RuO_2-Li_2S_6: The Li_2S_6 solution were prepared by dissolving and mixing stoichiometric amounts of Li_2S and sulfur in a molar ratio of 5 :1 in 1,3-dioxolane and 1,2-dimethoxyethane (v/v = 1:1) at 60℃ with stirring for 24 h. The chemical interaction between RuO_2 and lithium polysulfides was investigated by XPS. Typically, 20 mg of RuO_2@NMCs was placed in 10 mL of Li_2S_6 (2 mM) to obtain the RuO_2-Li_2S_6 solution. After settling for 12h, the precipitated RuO_2-Li_2S_6 product was dried for XPS analysis.

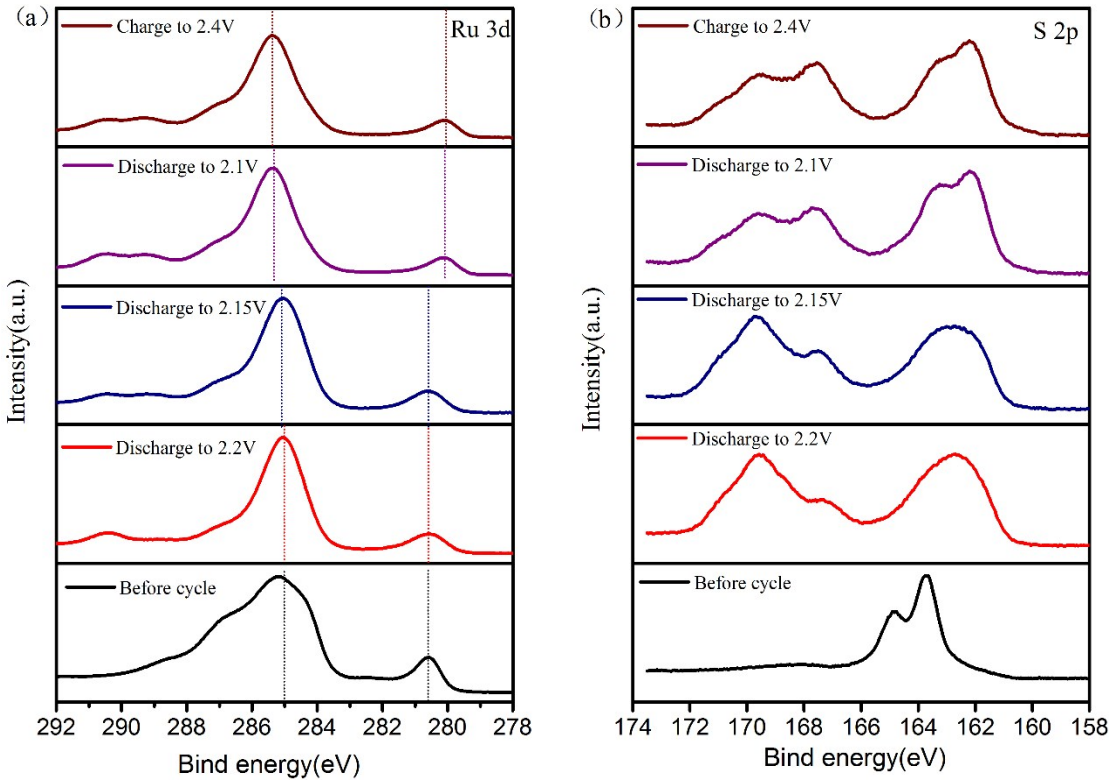

Figure S10. The *Ex*-situ XPS study on RuO_2@NMCs/S electrodes extracted from cells at different discharge states.

Table. S1. Comparisons of the cycling performance of this work with that of other composite cathodes from recent publications.

Composite materials	Initial discharge capacity (mAh g^{-1})	Cycle life	Current rate	Decay rate per cycle (%)
S/TiN[1]	988	500	0.5	0.07
S/Nb_2O_5[2]	1289	200	0.5	0.14
N-HPC-CNT/S [3]	622	600	1.0	0.07
MP-C/rGO/S [4]	919	500	1.0	0.073
MoS_2/rGO/S [5]	1159	600	0.5	0.083
S/CoO/HCN[6]	882	200	0.5	0.11
This work	1065	500	0.5	0.07

Supporting Reference

[1] Z. Cui, C. Zu, W. Zhou, A. Manthiram, J. B. Goodenough. Mesoporous titanium nitride-enabled highly stable lithium-sulfur batteries. *Adv. Mater.* 28 (2016) 6926-6931.

[2] Y. Tao, Y. Wei, Y. Liu, J. Wang, W. Qiao, L. Ling, D. Long. Kinetically-enhanced polysulfide redox reactions by Nb_2O_5 nanocrystals for high-rate lithium–sulfur battery. *Energy Environ. Sci.* 9 (2016) 3230-3239.

[3] Cai, J.; Wu, C.; Yang, S.; Zhu, Y.; Shen, P. K.; Zhang, K., Templated and Catalytic Fabrication of N-Doped Hierarchical Porous Carbon-Carbon Nanotube Hybrids as Host for Lithium-Sulfur Batteries. *ACS applied materials & interfaces* **2017,** *9* (39), 33876-33886.
[4] Qian, W.; Gao, Q.; Li, Z.; Tian, W.; Zhang, H.; Zhang, Q., Unusual Mesoporous Carbonaceous Matrix Loading with Sulfur as the Cathode of Lithium Sulfur Battery with Exceptionally Stable High Rate Performance. *ACS applied materials & interfaces* **2017,** *9* (34), 28366-28376.
[5] Lin, H.; Yang, L.; Jiang, X.; Li, G.; Zhang, T.; Yao, Q.; Zheng, G. W.; Lee, J. Y., Electrocatalysis of polysulfide conversion by sulfur-deficient MoS2 nanoflakes for lithium–sulfur batteries. *Energy & Environmental Science* **2017,** *10* (6), 1476-1486.
[6] Wu, S.; Wang, Y.; Na, S.; Chen, C.; Yu, T.; Wang, H.; Zang, H., Porous hollow carbon nanospheres embedded with well-dispersed cobalt monoxide nanocrystals as effective polysulfide reservoirs for high-rate and long-cycle lithium–sulfur batteries. *Journal of Materials Chemistry A* **2017,** *5* (33), 17352-17359.